

Nuclear Magnetic Resonance Chemical Shifts from Hybrid DFT QM/MM Calculations

Daniel Sebastiani^{*,†} and Ursula Rothlisberger[‡]

Max-Planck-Institute for Polymer Research, Ackermannweg 10, 55128 Mainz, Germany, and Institute of Molecular Chemistry and Biology, Ecole Polytechnique Fédérale de Lausanne, 1015 Lausanne, Switzerland

Received: August 14, 2003; In Final Form: January 6, 2004

We present a method to calculate NMR chemical shielding tensors in condensed phases by means of a hybrid quantum mechanical/molecular mechanical (QM/MM) approach. We propose a modification of the conventional QM/MM technique, adding a general repulsive potential to the electronic interaction Hamiltonian. This universal potential is motivated by the absence of Pauli repulsion in standard interaction potentials that are based only on classical point charges. We apply the method to realistic systems composed of molecules with strong dipolar character, thus forming strong hydrogen bond networks. In particular, we present calculations for liquid water and a proton conducting organic crystal. The electrical field and direct contact effects of surrounding molecules play a crucial role in the NMR resonance lines of such materials. The results are in very good agreement with full quantum calculations as well as with experiment. Thus, this new combination of *ab initio* NMR chemical shift calculations with a QM/MM modeling of extended systems provides an improved tool for the analysis of complex biological and chemical systems, such as polymers and proteins.

1. Introduction

Nuclear magnetic resonance (NMR) is a widespread analysis tool in many areas of chemistry and biology. One of the key quantities in this context are NMR chemical shift spectra, which allow the characterization of the chemical environment of individual atoms. In particular, bond types and interatomic distances can be obtained by analyzing the resonance frequencies of nuclear spins in an external magnetic field. NMR chemical shifts can also be used for measuring hydrogen bond strengths. Especially in condensed matter where hydrogen bonding ranges from intramolecular bridges up to complicated intermolecular networks, magic-angle-spinning (MAS) solid-state NMR has emerged in the past decade as a promising technique for the analysis of microscopic structures of molecular, macromolecular and supramolecular systems.¹

The strong dependence of the NMR chemical shift spectrum on the chemical environment of the considered atoms makes NMR a valuable tool for a unique characterization of microscopic structure. It allows the quantitative determination of many structural properties of locally ordered systems. Thus, it even provides information for materials that do *not* exhibit long-range order, and that are therefore problematic for conventional experimental methods.

For several years, the *ab initio* calculation of chemical shielding tensors has been a well-established method in quantum chemistry. Until recently, however, these calculations were always restricted to systems of finite size, i.e., molecules in the gas phase. Only for a few years have two methods been proposed for the treatment of the condensed phase, adopting periodic boundary conditions for the considered system.^{2,3} These approaches, developed in the framework of density functional theory (DFT)⁴ enable an analysis of the NMR chemical shifts

of many systems that could not be investigated before, such as crystalline and amorphous solids as well as liquids.^{5–9} In practice, these calculations can now be done on any system that is tractable with density functional theory-based computer codes imposing periodic boundary conditions.

In many cases, the calculation of NMR chemical shifts or other properties of a large system is not only prohibitively expensive but also not particularly interesting. Often, the chemically or biologically relevant parts are located in a small region, as in the case of a molecule in solution or the active site of an enzyme. In such cases, only this subsystem merits the computationally intensive treatment with quantum mechanical methods (QM) whereas the large remaining part of the system can be described with less accurate empirical molecular mechanics (MM) approaches.

A variety of methods to accomplish this task have been presented in the past decade. A review about this field is given in ref 10. One of the most recent implementations¹¹ interfaces the CHARMM force field code¹² with the Gaussian 98 suite of programs.¹³ This directly enables the calculation of NMR chemical shifts within the QM/MM framework for individual static configurations.

An alternative approach has been presented recently,¹⁴ which combines a classical force field (in this case from the GRO-MOS96¹⁵ or AMBER codes¹⁶) with a Car–Parrinello molecular dynamics package (CPMD^{17,18}). The CPMD package is based on a pseudopotential plane-wave scheme within density functional theory (DFT) under periodic boundary conditions. This hybrid QM/MM combination allows an efficient simulation of picosecond dynamics of extended systems such as solvated macromolecules or liquids, keeping the accuracy and flexibility of DFT while incorporating the ability to simulate explicitly all degrees of freedom of thousands of atoms.

This article focuses on the calculation of NMR chemical shifts within this framework. In particular, we shall investigate realistic systems in the condensed phase whose NMR chemical shifts have been computed under periodic boundary conditions within

[†] Max-Planck-Institute for Polymer Research. E-mail: sebastia@mip-mainz.mpg.de.

[‡] Ecole Polytechnique Fédérale de Lausanne. E-mail: ursula.rothlisberger@epfl.ch.

DFT by a recently presented method,^{3,19} and we compare them with analogous QM/MM calculations. We want to make sure that our method works well not only for model systems like small isolated molecular clusters but also for more complex geometries of real systems. Therefore, we take systems that do exist experimentally and that have already been investigated with both computational and experimental techniques. To evaluate the accuracy of the implementation, we compare these full-quantum shifts with our QM/MM calculations and evaluate the accuracy of the hybrid method.

In particular, we also want to test the reliability of the NMR chemical shift values of the border atoms of the QM subsystem. The NMR lines of those atoms that are close to or in direct contact with the classical part of the system are likely to be more difficult to describe. Their electrons see the QM fragment on one side, whereas the other side consists of a distribution of point charges, thus lacking any quantum-mechanical effects (e.g., Pauli repulsion).

To this purpose, we push the approach to its limits and investigate the results also for the case that only a *single molecule* is treated quantum mechanically, surrounded by a solvent or a given crystalline structure, described on the molecular mechanics level.

The extension to systems where covalent bonds cross the QM/MM boundary is in principle possible as well. However, this feature exceeds the scope of this article and will be presented in a future work.²⁰

2. Theory

2.1. NMR Chemical Shifts. In this section, only essentials of the computational method will be outlined, whereas detailed discussions of the NMR and the QM/MM implementation are published elsewhere.^{3,14}

The calculation of NMR chemical shifts is performed by density functional perturbation theory, using the methods described in refs 3 and 21. The DFT energy functional in the Kohn–Sham (KS) scheme,^{22,23} denoted by ϵ_{KS} , is modified by an additional term ϵ_{B} , which describes the effect of an external magnetic field \mathbf{B} . The additional contribution is very small compared to ϵ_{KS} and can therefore be treated perturbatively:

$$\epsilon_{\text{KS}} \rightarrow \epsilon_{\text{KS}} + \epsilon_{\text{B}} \quad (1)$$

Equation 1 is expanded in powers of the perturbation, i.e., in the strength B of the magnetic field:

$$\epsilon_{\text{KS}} + \epsilon_{\text{B}} = \epsilon^{(0)} + B\epsilon^{(1)} + \frac{1}{2}B^2\epsilon^{(2)} + \dots \quad (2)$$

The variational principle is applied to all orders that arise from the expansion.²¹ At zero order, this formalism yields the usual Kohn–Sham equations:

$$\hat{\mathbf{H}}^{(0)}|\varphi_i^{(0)}\rangle = \epsilon_i|\varphi_i^{(0)}\rangle \quad (3)$$

with the KS–Hamiltonian $\hat{\mathbf{H}}^{(0)}$, its energy eigenvalues ϵ_i , and the corresponding unperturbed Kohn–Sham orbitals $\varphi_i^{(0)}$. The expansion of the Hamiltonian and the orbitals is done in complete analogy to eq 2:

$$\hat{\mathbf{H}} = \hat{\mathbf{H}}^{(0)} + B\hat{\mathbf{H}}^{(1)} + \frac{1}{2}B^2\hat{\mathbf{H}}^{(2)} \quad (4)$$

$$|\varphi_i\rangle = |\varphi_i^{(0)}\rangle + B|\varphi_i^{(1)}\rangle + \frac{1}{2}B^2|\varphi_i^{(2)}\rangle + \dots \quad (5)$$

The second-order expansion of the energy functional results in a linear equation (eq 34 of ref 3) for the wave function components $\varphi_i^{(1)}$, which are first order in the magnetic field:

$$\sum_j (\hat{\mathbf{H}}^{(0)}\delta_{ij} - \epsilon_{ij})|\varphi_j^{(1)}\rangle = -\hat{\mathbf{H}}^{(1)}|\varphi_i^{(0)}\rangle \quad (6)$$

$$\epsilon_{ij} = \langle \varphi_j^{(0)} | \hat{\mathbf{H}}^{(1)} | \varphi_i^{(0)} \rangle \quad (7)$$

where $\hat{\mathbf{H}}^{(1)}$ is the perturbation Hamiltonian. In the original formulation of ref 21, $\hat{\mathbf{H}}^{(1)}|\varphi_i^{(0)}\rangle$ was written as the derivative of a perturbation functional ϵ_{B} with respect to the KS orbitals. In the case of a finite molecular system, it is given by

$$\hat{\mathbf{H}}^{(1)} = \frac{1}{2c}(\hat{\mathbf{r}} - \mathbf{R}_{\text{g}}) \times \hat{\mathbf{p}} \quad (8)$$

with the gauge origin \mathbf{R}_{g} defining the origin of the coordinate system for the position operator $\hat{\mathbf{r}}$. Although the actual value of \mathbf{R}_{g} is in principle arbitrary, in practice it is crucial to tune it to minimize numerical errors due to the incompleteness of the basis set in an actual calculation. In quantum chemistry, several methods exist to optimize the choice for the gauge origin,^{24–26} which have all been shown to yield reliable results. In our approach, the continuous set of gauge transformations (CSGT) method is applied,²⁶ in which the gauge origin is continuously set equal to the point in space at which the induced current density (see below, eq 9) is computed.

The gauge problem is not affected by the presence of the external potential of the MM atoms. From the view of the magnetic linear response calculation, the only effect of the MM system is the change in the local electrostatic potential.

In the case of condensed phase systems a further complication arises due to the fact that the position operator $\hat{\mathbf{r}}$ is ill-defined in periodic boundary conditions. As shown in ref 3, a possible solution is the introduction of a new orbital-dependent saw-tooth-shaped position operator $\hat{\mathbf{r}}$. To eliminate the effects of the unphysical jump in the saw-tooth operator, maximally localized Wannier orbitals²⁷ have to be used in combination with this technique. A more detailed discussion on the realization of this method for magnetic fields under periodic boundary conditions can be found in refs 3, 19, and 28.

Both the unperturbed and perturbed DFT equations, eqs 3 and 6, are self-consistently solved by means of iterative algorithms, yielding the sets of wave functions $|\varphi^{(0)}\rangle$ and $|\varphi^{(1)}\rangle$, respectively. Subsequently, the quantum-mechanical current density is computed from these orbitals:

$$\mathbf{j}(\mathbf{r}) = \frac{1}{2c} \sum_i [\varphi_i^{(0)*}(\mathbf{r}) \hat{\mathbf{p}} \varphi_i^{(1)}(\mathbf{r}) - \varphi_i^{(1)*}(\mathbf{r}) \hat{\mathbf{p}} \varphi_i^{(0)}(\mathbf{r})] \quad (9)$$

This electronic current density can readily be used to obtain the induced magnetic field through

$$\mathbf{B}^{\text{ind}}(\mathbf{r}) = \frac{1}{c} \int d^3\mathbf{r}' \frac{\mathbf{r} - \mathbf{r}'}{|\mathbf{r} - \mathbf{r}'|^3} \times \mathbf{j}(\mathbf{r}') \quad (10)$$

$$= -\frac{1}{c} \nabla \times \int d^3\mathbf{r}' \frac{\mathbf{j}(\mathbf{r}')}{|\mathbf{r} - \mathbf{r}'|} \quad (11)$$

For a given direction of the externally applied magnetic field,

the induced field at the position of a nucleus $\mathbf{B}^{\text{ind}}(\mathbf{R}_I)$ defines one row of the chemical shielding tensor $\sigma(I)$ of the atom I :

$$\sigma_{\alpha\beta}(I) = -\frac{\partial \mathbf{B}_{\alpha}^{\text{ind}}(\mathbf{R}_I)}{\partial \mathbf{B}_{\beta}^{\text{ext}}} \quad (12)$$

In experiment, the trace of the shielding tensor of the species of interest X is measured relative to a certain reference substance:

$$\delta(X) = \text{Tr } \sigma(\text{ref}) - \text{Tr } \sigma(X) \quad (13)$$

We follow this experimental convention and cite the trace of the shift tensor, with respect to the considered molecule placed in vacuo.

2.2. Hybrid QM/MM Modeling. We now switch to the second part of the method, the inclusion of a large surrounding atomistic system that is described by empirical parameters instead of an electronic structure approach.

In most QM/MM schemes, the interaction of the classical atoms with the quantum part is described by means of an external field that is added to the quantum Hamiltonian. In our approach, this field represents the effects of point charges placed at the positions of the classical atoms.

The implementation of the QM/MM interaction Hamiltonian into an electronic structure calculation scheme has the effect of polarizing the quantum system by means of the electrostatic field of the classical point charges. Both the ground-state Kohn–Sham orbitals as well as the spectroscopic properties of the system will be affected by this polarization.

It follows from the Hohenberg–Kohn theorem that the change in the electrostatic potential due to the additional classical field will result in new KS orbitals and a different electronic density. Together with a suitable interaction scheme for the QM/MM interface region, this is the basic ingredient for the total energy calculation.¹⁴

In addition, the perturbation theory equations themselves are modified. Both the unperturbed Hamiltonian $\hat{\mathbf{H}}^{(0)}$, its matrix elements eq 7 and the unperturbed KS orbitals $|\varphi^{(0)}\rangle$ must be replaced by those of the QM/MM calculation. After substitution into eq 6, the new linear response orbitals $|\varphi^{(1)}\rangle$ can readily be inserted into the formula for the induced current density, eq 9. Finally, the induced magnetic field is given by eq 11, yielding the NMR chemical shielding tensors, eq 12, within the QM/MM framework.

The central issue in hybrid quantum-classical (QM/MM) calculations concerns the question how exactly the quantum and the classical subsystems are interfaced. A variety of approaches has been proposed to treat this problem.¹⁰

In the method presented here, the quantum part is enclosed into a box of finite volume, in which the Kohn–Sham equations are solved, using a plane-wave basis set under periodic boundary conditions. To avoid interactions with the periodic images, an appropriate screening technique is used²⁹ to eliminate the effect of the periodic replicas of the quantum box. The interaction of the quantum system with the classical atoms is mediated by the electrostatic potential created by the point charges. The classical system itself is also described using periodic boundary conditions.

The corresponding interaction energy has the following form:

$$E_{\text{QM/MM}} = \sum_{I \in \text{MM}} \int_{\Omega} d^3r \rho(\mathbf{r}) v_I(|\mathbf{r} - \mathbf{R}_I|) \quad (14)$$

where the integral runs over the quantum cell Ω , with the

electronic and ionic charge density $\rho(\mathbf{r})$, the positions \mathbf{R}_I of the classical atoms I , and a pseudopotential-like Coulomb potential $v_I(\mathbf{r})$. This potential follows the normal electrostatic potential of the point charges at long range, whereas at short distances, its singularity is smoothed. This is done to suppress the unphysical electron spill-out effect, which is particularly problematic for delocalized basis sets such as plane waves. To this purpose, the following form has been suggested¹⁴ for $v_I(\mathbf{r})$:

$$v_I(r) = q_I \frac{r_{\text{c},I}^n - r^n}{r_{\text{c},I}^{n+1} - r^{n+1}} \quad (15)$$

An exponent of $n = 4$ and a radial parameter $r_{\text{c},I}$ equal to the covalent radius of the atom I were chosen in the original work, but other possibilities are also tested in this article. A variation of eq 15 is given by

$$v_I(r) = q_I \frac{r^m}{\sqrt{r_{\text{c},I}^{2m+2} - r^{2m+2}}} \quad (16)$$

In this choice, where typically $m = 1$ or $m = 2$, the Coulomb potential vanishes near the position of the classical atom. This feature prevents electrons from spreading from the quantum part into the region with classical atoms due to their attractive Coulomb potentials. In reality, this phenomenon is forbidden due to the electronic Pauli repulsion of surrounding classical atoms, but because those electrons are not considered explicitly in a QM/MM calculation, the repulsive effect is absent.

This Pauli repulsion can be represented even more explicitly, by means of an additional short-ranged potential of exponential or Gaussian type. This potential is superimposed to the smoothed Coulomb potential of the classical point charges and should be exclusively repulsive in nature. Thus, the total QM/MM interaction potential reads

$$v_I(r) = q_I \frac{r^m}{\sqrt{r_{\text{c},I}^{2m+2} - r^{2m+2}}} + v_0 e^{-(r/r_{\text{rep}})^k} \quad (17)$$

with an additional “repulsive radius” r_{rep} and an exponent of $k = 1$ or $k = 2$.

The effect of such an additional repulsive potential is discussed in detail in the following sections. Its main purpose is to mimic the orthogonality constraint that would be imposed on the electrons if also the MM region was treated quantum mechanically. Therefore, the decay radius r_{rep} should coincide with the spatial extent of the valence electron wave functions of the considered nucleus. As for the cutoff radius $r_{\text{c},I}$ of the Coulomb potential, a natural choice for r_{rep} is the covalent radius r_{cov} of the atom.

Similar ideas for compensating the short-ranged Pauli repulsion have already been realized in the context of continuum solvation models^{30,31} and QM/MM implementations,³² as well as in the effective fragment potential method.³³ Yang and co-workers used a special monovalent pseudopotential³⁴ replacing the first MM atom that can also effectively mimic Pauli repulsion.

The short-range potential represents an additional repulsive interaction between the MM atoms and the QM electrons. This interaction would create new repulsive atomic forces (mediated by the electrons) between the MM part and the QM atoms in the QM/MM border region. Such forces are in principle already taken into account in the classical van der Waals potential

between QM and MM atoms. Thus, there is a double-counting of this interaction that could significantly influence the geometry of the system. However, in the present work, this problem is circumvented by using the new potential only a posteriori, i.e., on geometries that have been obtained without it. The inclusion of our Pauli potential into a molecular dynamics simulation, which would require a careful analysis of this double-counting problem, and probably the omission of the standard van der Waals r^{-12} repulsion between the QM and MM atoms, is beyond the scope of this article.

3. Computational Details

To gauge the performance of the QM/MM approach, we compare the results of a full DFT calculation with the corresponding QM/MM result. The aim of hybrid methods being the description of large disordered systems, it is desirable to choose a system that naturally exhibits a broad variety of individual microscopic structures. Model systems containing only a small number of molecules are valuable for a first estimate, but they are too restricted to account for the large range of microconfigurations that can be found in real systems. On the other hand, large molecular cluster models quickly exceed the size that quantum chemical calculations can deal with.

As a compromise, we consider a snapshot from an *ab initio* Car–Parrinello molecular dynamics simulation of liquid water³⁵ at ambient conditions. The simulation was done under periodic boundary conditions, using a supercell with 64 water molecules. The use of a periodic box avoids surface effects, from which a cluster calculation naturally suffers. It has also been shown that size effects are already negligible at this system size.³⁵ The simulation temperature was kept within a small window around 300 K, to let the system perform an efficient sampling of phase space. Already within a single molecular dynamics snapshot, a large range of microconfigurations can be found. The challenge for the QM/MM implementation is now to correctly describe the ensemble of individual configurations and to yield accurate NMR chemical shifts of the individual atoms of this system.

The NMR chemical shielding tensors of all atoms of this system were computed fully from first principles, by means of the method presented in ref 3. The approach has been shown to agree well with experiment, in particular for water in normal and supercritical states.⁷ As in the molecular dynamics simulation, a cutoff of 70 Ry was used for the calculation of the NMR parameters, and the core electrons were modeled by pseudopotentials of the Goedecker type.³⁶ Because the BLYP exchange–correlation functional has been shown to describe the hydrogen bond network within the considered water system with good accuracy,³⁷ this functional was also chosen here. As a reference system for the chemical shifts according to eq 13, an isolated water molecule was taken. It was fully relaxed with the same computational setup as used in the molecular dynamics simulation.

The chemical shift values obtained this way are compared to calculations within the QM/MM framework. To this purpose, a separate setup was done for each water molecule, which defines the center of the QM subsystem. In a first calculation, only the considered molecule was described by QM, whereas in a second and third run, all water molecules within solvation spheres of $d_{OO} \leq 3.5$ Å and $d_{OO} \leq 5.0$ Å were included in the quantum region, as illustrated in Figure 1. These criteria correspond to the first and second minimum of the O–O pair correlation function.³⁵ The surrounding water molecules were modeled by standard point charges (SPC model, $q_O = -0.82e$ and $q_H = +0.41e$), interacting through eqs 15–17 with the



Figure 1. Cluster of a water molecule surrounded by its first solvation shell, and the remaining water molecules which are modeled classically.

quantum box. The atomic coordinates were not modified with respect to the *ab initio* simulation.

Naturally, as the size of the QM subsystem increases, the full-quantum shifts must be approached. However, the question of interest is how much the presence of the classical point charges can improve a calculation of a small cluster of few quantum molecules only. The degree of improvement can be quantified by the root-mean-square (rms) deviation Δ of the chemical shifts:

$$\Delta = \left(\frac{1}{N} \sum_i (\delta_{\text{fullQM}}^H - \delta_{\text{QM/MM}}^H)^2 \right)^{1/2} \quad (18)$$

We denote this deviation by Δ to avoid confusion with the shielding tensor, σ .

4. Proton Chemical Shifts in Liquid Water

Water in its liquid state is the most important biological solvent on our planet and has therefore attracted special interest for decades. Its properties, in particular the unusually strong and fluctuating hydrogen bond network, has been the subject of a series of investigations in recent times. A necessarily incomplete selection of theoretical and experimental investigations can be found in refs 7, 8, 35, and 38–45.

4.1. Single Quantum Molecule. As a first step, a solvated water molecule is modeled as an isolated particle, with and without the surrounding classical molecules. The QM calculation of a single water molecule, with or without a classical solvation shell, cannot adequately reproduce the electronic structure that would exist in the presence of a realistic hydrogen bond network. Thus, the chemical shift values will agree only qualitatively with the true liquid-state calculation. But although this setup represents a relatively crude approximation, it allows surprising insight into the nature of aqueous solvation.

The correlation of the proton NMR chemical shifts of the 128 hydrogen atoms between the full quantum calculation and the cluster and QM/MM results are shown graphically in the top of Figure 2. A quantitative benchmark is given by means of the rms deviations according to eq 18 in Table 1. Not surprisingly, the isolated water molecule performs worst. However, also the addition of point charges, according to eq

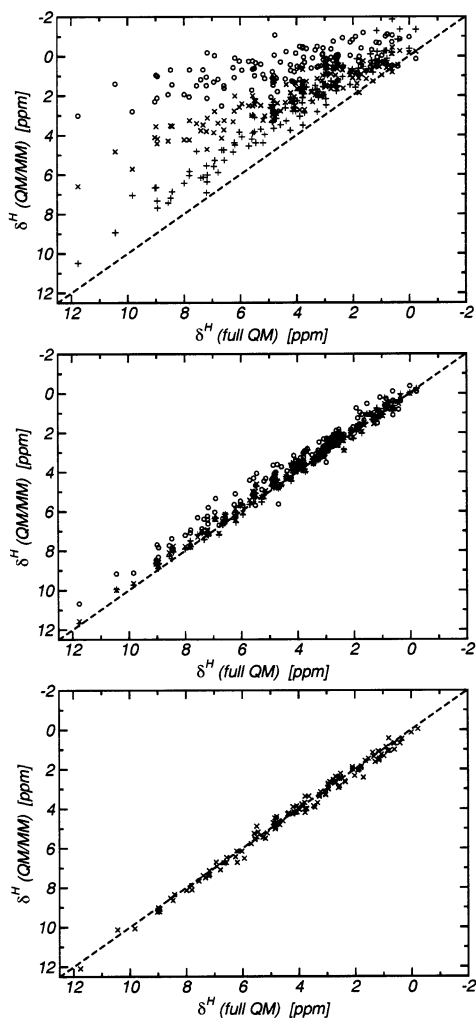


Figure 2. Correlation of the isotropic ^1H NMR chemical shifts between QM/MM and full QM calculations. Only a single molecule (top), a molecule with its first solvation shell defined by $d_{\text{OO}} \leq 3.5 \text{ \AA}$ (middle), and a molecule with its second solvation shell ($d_{\text{OO}} \leq 5 \text{ \AA}$, bottom) are described as QM. Circles represent the isolated molecule alone, the crosses stand for a QM/MM description according to eq 16, and the plus symbols show the effect of the additional repulsive potential, eq 17. The dashed line (optimal correlation) is a guide for the eye.

TABLE 1: RMS Deviation Δ_H in ppm of the QM/MM ^1H NMR Chemical Shift Results for Liquid Water with Respect to the Full QM Values^a

QM region	isolated cluster	QM/MM	
		w/o v_{rep}	w/ v_{rep}
single molecule	0.37	0.23	0.137
molecule with first solvation shell ($d_{\text{OO}} \leq 3.5 \text{ \AA}$)	0.06	0.028	0.028
molecule with second solvation shell ($d_{\text{OO}} \leq 5 \text{ \AA}$)		0.021	

^a Different methods are used for taking into account the interaction with the solvent molecules. The parameters for the repulsive potential are $k = 2$, $v_0 = 2 \text{ au}$, and $r_{\text{rep}} = 1.2 r_{\text{cov}}$.

15, yields only a moderate result. The modified expression for the smoothed Coulomb singularity, eq 16, shows no significant difference compared to the potential of eq 15. Instead, the inclusion of an explicit repulsive term in the classical potential by means of eq 17 improves the quality of the shifts dramatically. The data shown in Figure 2 was obtained using $m = 1$, $k = 2$, $v_0 = 2.0 \text{ au}$, and $r_{\text{rep}} = 1.2 r_{\text{cov}}$.

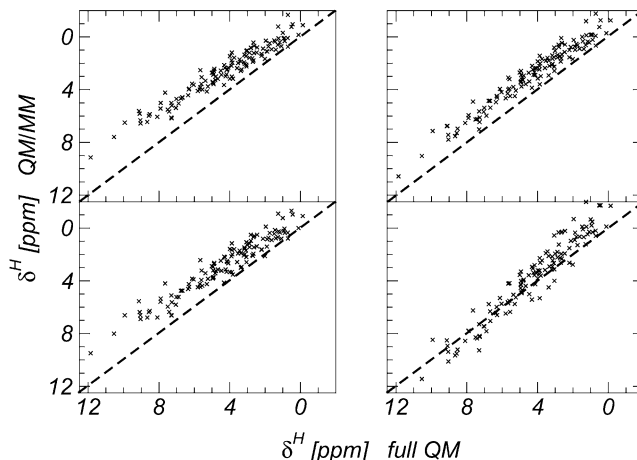


Figure 3. Effect of the parameters k , v_0 , and r_{rep} in the repulsive potential, eq 17, on the ^1H NMR chemical shifts in the QM/MM calculation of the single molecule. Left: $k = 1$, $v_0 = 3 \text{ au}$, $r_{\text{rep}} = 0.6$, r_{cov} (top); $k = 1$, $v_0 = 2 \text{ au}$, $r_{\text{rep}} = 0.8$, r_{cov} (bottom). Right: $k = 2$, $v_0 = 2 \text{ au}$, $r_{\text{rep}} = 1.2$, r_{cov} (top); $k = 2$, $v_0 = 1 \text{ au}$, $r_{\text{rep}} = 1.41$, r_{cov} (bottom).

A more detailed analysis of the dependence of the shifts on these parameters is shown in Figure 3. Among the variety of the possible values that we have tested, only a few selected combinations are shown. The various parameters all yield similar shift correlations.

4.2. First Solvation Sphere. When the first solvation shell is added to the quantum box, the hydrogen bonding structure of the central water molecule becomes much more similar to that of the true extended system. Thus, the requirement for the additional repulsive potential becomes weaker. However, a finite cluster of atoms will lack important features of the extended system, which have to be accounted for by means of the QM/MM point charges.

We have computed the ^1H NMR chemical shift values in this configuration, with and without the QM/MM charges and the repulsive potential. To calculate the proton shifts of a given molecule, all neighboring water molecules within the first solvation shell, defined by the first minimum of the oxygen–oxygen pair correlation function around $d_{\text{OO}} = 3.5 \text{ \AA}$,³⁷ were included in the quantum region.

The results are shown in the middle graph of Figure 2. Although already the isolated clusters give reasonable results, the incorporation of second neighbor solvent effects by means of the point charges yields a significantly better correlation with the full quantum calculation. The rms deviations in Table 1 show that the QM/MM description results in a significant improvement with respect to the isolated cluster calculation.

4.3. Second Solvation Sphere. The inclusion of all water molecules from the second solvation shell further improves the description of the hydrogen bond network and the electrostatic field for the central molecule. This model leads to an agreement with the fully periodic NMR calculation that lies within the numerical accuracy of the method. In the bottom graph of Figure 2, the correlation with the full QM calculation is shown, and the rms deviation is given in Table 1.

The change in the rms deviation with respect to the smaller water cluster is only 0.007, elucidating that the NMR chemical shift is a very local property. It is almost unaffected by changes in the chemical environment, which are more than 5 \AA away from the considered nuclear spin.

It turns out that there is an almost regular improvement by a factor of 2 in the rms deviations in the sequence isolated QM

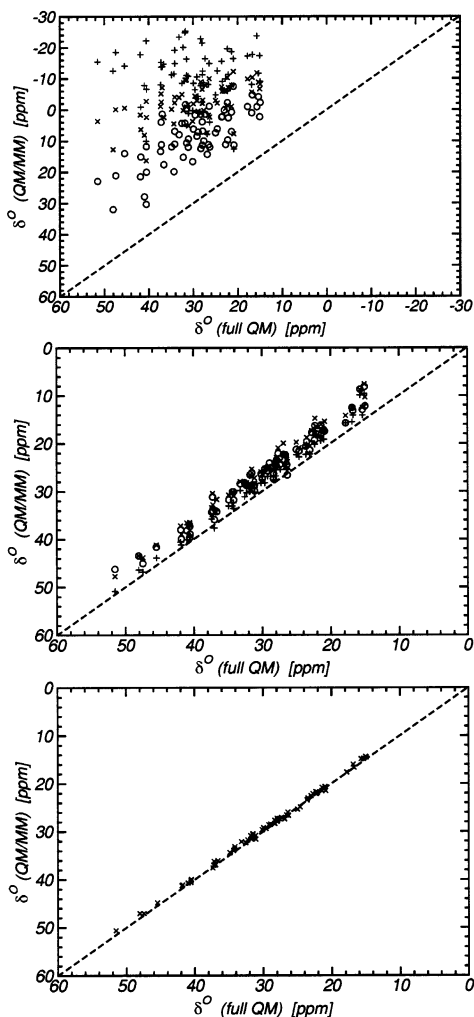


Figure 4. Correlation of the isotropic ^{17}O NMR shifts with the fully periodic QM calculation: (top) isolated water molecule; (middle) water cluster (first solvation shell); (bottom) water molecule with the first two solvation shells. Only the QM/MM calculation without repulsive potential is shown in the bottom graph. The symbols have the same meanings as in Figure 2. The NMR chemical shieldings were referenced to the shielding of an isolated, optimized water molecule.

molecule \rightarrow QM molecule with MM \rightarrow QM/MM with repulsive potential \rightarrow isolated first solvation shell QM \rightarrow solvation shell QM with MM.

5. Oxygen Chemical Shifts in Liquid Water

5.1. Single Quantum Molecule. The oxygen NMR chemical shifts are automatically obtained from the calculation. Physically, they suffer from the use of pseudopotentials, which limits their accuracy to some extent.⁴⁶ However, tendencies and relative differences are reproduced with good accuracy. Thus, it makes sense to investigate in how far the solvent shifts may already be obtained by using classical point charges.

The minimalistic procedure, which consists of taking an isolated molecule, is shown in the top graph of Figure 4. Surprisingly, the inclusion of classical charges and also the short-sighted repulsive potential *deteriorate* the NMR chemical shifts of the oxygen atom. To our knowledge, no combination of classical charges and repulsive parameters has been found so far that would improve this behavior. However, it is consistent with the recent QM/MM work of Cui et al.,¹¹ in which they also find a wrong sign for the tendency of the oxygen NMR chemical shift of water dimers at close distances (Figure 1 of

TABLE 2: RMS Deviation Δ_0 in ppm of the QM/MM ^{17}O NMR Chemical Shift Results for Liquid Water with Respect to the Full QM Values^a

QM region	isolated cluster	QM/MM	
		w/o v_{rep}	w/ v_{rep}
single molecule	2.77	4.12	5.37
molecule with first solvation shell ($d_{\text{OO}} \leq 3.5 \text{ \AA}$)	0.48	0.57	0.31
molecule with second solvation shell ($d_{\text{OO}} \leq 5 \text{ \AA}$)		0.07	

^a The parameters for the repulsive potential are $k = 2$, $v_0 = 2 \text{ au}$, and $r_{\text{rep}} = 1.2 r_{\text{cov}}$.

ref 11). They do not discuss this point in detail, and they also do not investigate water dimers with more than one strong hydrogen bond, which are present in our liquid water snapshots. In those geometries, where several protons have H-bonds to an acceptor oxygen, it seems that the QM/MM description does not yet work very well. It results in an overshielding instead of a deshielding of the oxygen.

This problem is unsolved at present and subject to ongoing research. The molecular electronic structure of the lone pairs of the oxygen do not respond correctly to the external potential of the MM charges. Also, the repulsive short-sighted potential seems not to be sufficient to rectify this situation. Further possible reasons for this behavior (e.g., missing polarization of the classical force field, geometric relaxation effects, etc.) are currently under investigation. Thus, QM/MM oxygen NMR chemical shifts should be analyzed with great care if the oxygen is close to classical atoms.

5.2. First Solvation Sphere. The incorporation of the first solvation sphere, i.e., molecules with $d_{\text{OO}} \leq 3.5 \text{ \AA}$, inverses the behavior found in the previous paragraph. The data are shown in the middle graph of Figure 4. The isolated cluster calculation already performs reasonably well, as does the QM/MM description. The combination with the repulsive potential further improves the results significantly. Even though in the graph, the differences are not clearly visible, the rms deviation (given in Table 2) is clearly improved in the case of the QM/MM calculation containing the repulsive potential. This indicates that the polarization due to the surrounding solvent is still visible to the central water molecule. It also supports the general justification of the repulsive potential, despite its inadequate effect for the single QM molecule.

5.3. Second Solvation Sphere. As in the case of the proton NMR chemical shifts, the cluster containing all molecules within $d_{\text{OO}} \leq 5 \text{ \AA}$ yield an almost perfect agreement with the fully periodic QM calculation (bottom of Figure 4). The calculation is relatively expensive, because, for each water molecule under consideration, a system of typically 24 solvation molecules has to be computed. Therefore, only the QM/MM calculation was done for the whole set of molecules, and only several test calculations were performed to check that the isolated cluster calculation as well as the repulsive potential have a negligible effect on the chemical shifts.

The rms deviation is naturally better than for the systems with smaller QM regions (see Table 2), but of course also the computational effort is considerably higher, as discussed below.

6. Computational Resources

An important practical aspect of numerical calculations is the required computational resources, in particular the CPU time necessary to obtain a certain result. In Table 3, we have listed the total time that is needed for the calculation of all NMR chemical shifts of the 64-molecules liquid water system.

TABLE 3: Approximate CPU Times in Processor Hours of the NMR Chemical Shift Calculations for the Liquid Water System, as a Function of the Size of the Quantum Region^a

QM region	6-311++G(p,d)	plane-wave 70 Ry
single molecule	0.05	0.2
molecule + 3.5 Å solvation shell	0.45	1.5
molecule + 5.0 Å solvation shell	19	11
full periodic QM	n/a	300

^a We show the total time that is required for one NMR calculation (number of hours \times number of processors).

There are two competing approaches that are possible for an isolated cluster calculation, using either localized basis sets (often Slater-orbital or Gaussian-type) or a plane wave basis in connection with a pseudopotential approach. An important issue for benchmarks is of course the basis set size. Unfortunately, there is no direct way of converting a localized basis of a certain quality, characterized by the number of (contracted) Gaussian functions, into a plane wave basis set of the same quality, which is characterized by an energy cutoff.

A further fundamental difference between the two basis sets is that the Gaussian functions represent an all-electron basis, whereas in the plane-wave approach, the core electrons are incorporated into the effective core potentials of the nuclei. Thus, only the valence electrons are treated explicitly, reducing the computational cost of the method. Moreover, all program packages perform differently in terms of efficiency for different systems. Therefore, there is no way of comparing two calculations with these different approaches in a “fair” and objective way.

We have tried, however, to compare similarly converged basis sets, using a standard localized basis with additional diffuse and polarization functions and a well converged plane wave basis with a cutoff of 70 Rydberg.

The reference calculations with the localized 6-311++G(d,p) basis set were done with a standard quantum chemistry program, whereas all other calculations were undertaken with the CPMD code.¹⁸

The latter code is also parallelized, enabling a parallel execution on a home-built 16-processor beowulf cluster. The benchmarks were done on standard Pentium-4 machines with 2 GHz clock speed.

The two kinds of basis sets show a qualitatively different scaling with the size of the problem. The isolated water molecule can be calculated almost instantaneously by the localized basis set, whereas the plane wave calculation requires a relatively long time. This is due to the fact that in plane-wave codes, an isolated system has to be placed within a real-space box of a certain minimum size, which contains mostly vacuum but which has to be included in the calculation nevertheless. This is due to the fact that the electronic wave functions have to be allowed to decay toward the borders of the cell in which the system is placed. An increase of this (mostly empty) unit cell at fixed cutoff energy results in an enlargement of the plane wave basis, which in turn increases the memory and CPU time requirements. This complication is absent when using localized basis sets.

In contrast, if the system becomes larger, less of the volume is occupied by vacuum and the relative computational effort changes significantly.

At the level of the first solvation shell (which results in a system of about 20 atoms), the localized basis set is clearly advantageous, but for more than about 50 atoms, the break-even point in favor of the plane-wave calculations is reached.

A typical QM/MM simulation of a realistic biochemical system easily exceeds this efficiency threshold.⁴⁷ Furthermore, the plane wave basis is free of any basis set superposition error, which was not taken into account in the calculations with the localized basis, but which can have a significant impact on the overall time and complexity.

However, the inverse is true for the case of a QM system that is not dense packed in space but more spread out. Then, the QM box of a plane wave calculation would contain mostly empty space, making it comparably inefficient. Thus, the break-even point mentioned here is of rather qualitative nature and may be different for other types of systems.

The convergence of the SCF cycle in the plane-wave approach is slightly influenced by the presence of the repulsive potential. Being very localized, it contains components of large reciprocal space vectors (**G** vectors), thus somewhat slowing down the wave function optimization. However, we found that the difference in CPU time between QM/MM calculations with and without the repulsive potential is of the same order of magnitude as the fluctuations between the snapshots. In the absence of any classical potential, the required number of SCF cycles for both the ground-state and the perturbation theory optimizations is about 10–30% smaller.

7. Crystalline Imidazole-Ethyleneoxide

An important question in the development of ab initio related methods is the transferability of the proposed schemes. We have therefore applied the QM/MM NMR chemical shift method to another system with a different chemical composition, to check whether the scheme of the repulsive short-ranged potential according to eq 17 is universally valid.

We have chosen imidazole-polyethylene-imidazole ($\text{N}_2\text{C}_3\text{H}_3\text{—}(\text{CH}_2\text{OCH}_2)_3\text{—N}_2\text{C}_3\text{H}_3$), a hydrogen-bonded crystal that has recently been investigated experimentally and theoretically,^{9,19} as a further test case. Due to its high anisotropic proton mobility, combined with its thermal stability and chemical robustness with respect to poisoning by carbon monoxide, this material is a candidate for fuel cell membranes. The crystalline unit cell contains two inequivalent molecules, which form a hydrogen bonded pair. This pair is linked to other pairs by further hydrogen bonds. Besides various packing effects, its ¹H NMR chemical shift spectrum therefore shows two downfield resonances (at 14.5 and 16.5 ppm), which have experimentally and theoretically been assigned to two different types of strong $\text{NH}\cdots\text{N}$ hydrogen bonds.⁹ In the experimental spectrum, there is one more peak (at 10.5–12 ppm) which is assigned to mobile protons in the system. These protons are most probably located in noncrystalline domains of the particular sample studied in this experiment.

For the QM/MM NMR calculation, we have taken a single molecule into the quantum box, as sketched in Figure 6. The remaining part of the crystal was treated classically, using point charges obtained by the standard restrained electrostatic potential fitting procedure (RESP) according to ref 48. For the additional repulsive potential in eq 17, we used the same values as for the liquid water system ($m = 1$, $k = 2$, $v_0 = 2$ au, and $r_{\text{rep}} = 1.2r_{\text{cov}}$).

The results are shown in Figure 5. Clearly, the QM/MM scheme without repulsive potential results in a misinterpretation of the peak at 10.5–12 ppm, because the latter should be absent in a perfect crystal. The downfield peaks at 14.5 ppm and 16.5 ppm are not found at all in the calculation. However, upon addition of the short-range repulsive potential, the chemical shifts of the nitrogen protons move to the right position at about 15 ppm, although they are not resolved as much as in the full

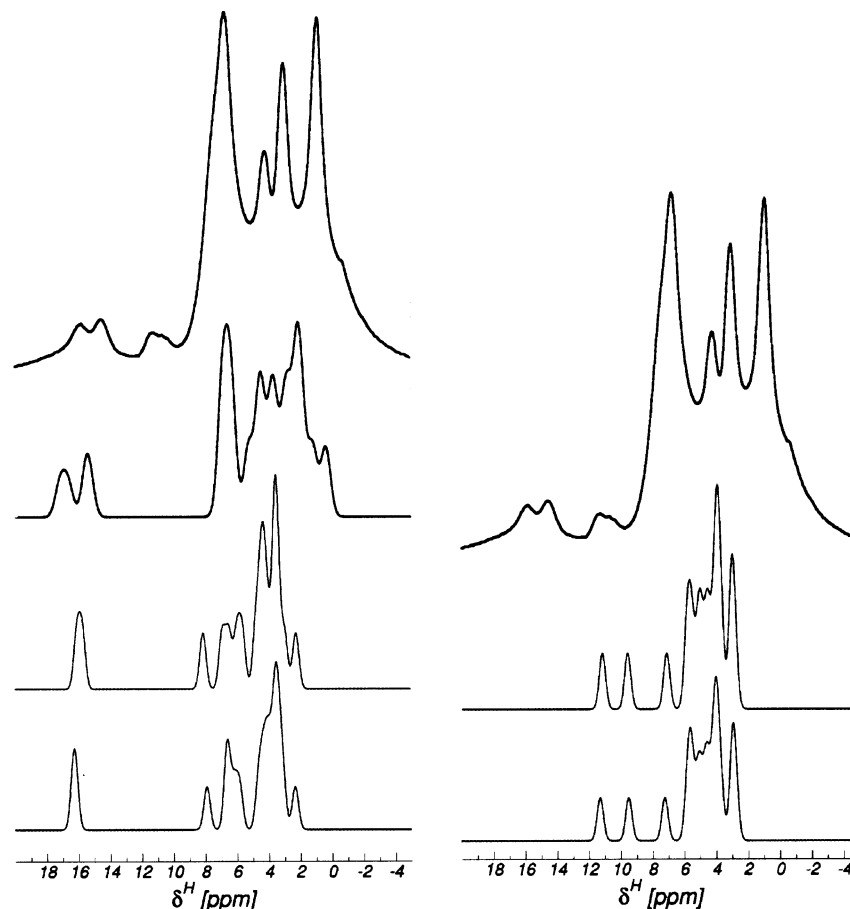


Figure 5. ^1H NMR spectra of the imidazole-poly(ethylene oxide) crystal. Left, from top to bottom: experimental solid-state spectrum, full QM calculation, QM/MM calculations *with* the repulsive potential according to eq 17. Right, from top to bottom: experimental solid-state spectrum, single molecule QM/MM calculations *without* the repulsive potential. The four bottom graphs (gray) represent the two crystallographically different molecules, which were computed separately.

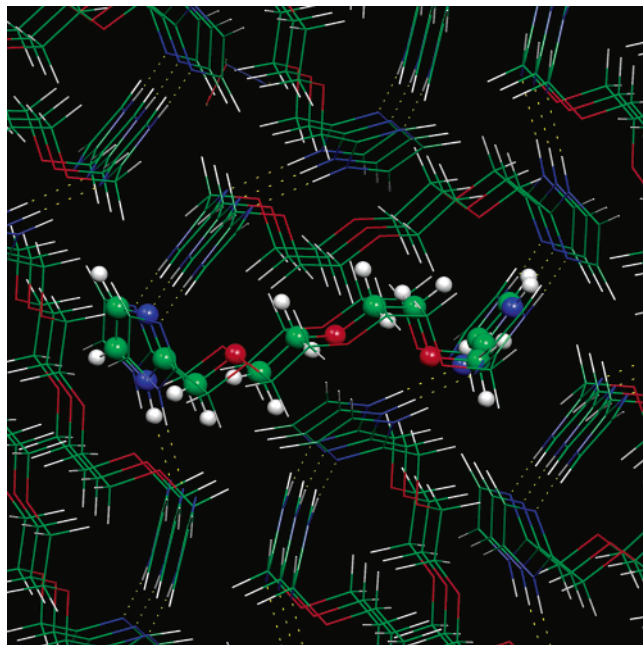


Figure 6. Crystal structure of Imi-2-EO. The QM molecule is drawn plainly, with the surrounding MM neighbors as thin lines.

quantum-mechanical spectrum. However, the improvement with respect to the straightforward QM/MM model is considerable.

Thus, also in this system, the repulsive potential is able to correct for a good part of those effects that are neglected in the conventional QM/MM description.

8. Conclusion

We have presented an analysis of ab initio calculations of the proton and oxygen NMR chemical shifts of liquid water, and the proton chemical shifts of an imidazole-poly(ethylene oxide)-imidazole crystal within a combination of recently developed QM/MM and linear response methods for systems in the condensed phase. We demonstrate that the standard classical/quantum interaction through smoothed point charges indeed helps to reproduce the NMR chemical shifts in a satisfying way. However, the Pauli repulsion from the electronic orbitals of the classically modeled atoms can be crucial but is not taken into account in the QM/MM method.

A suitable additional short-ranged repulsive potential of a simple Gaussian shape improves the NMR chemical shift results significantly. The potential pushes the electrons out of those regions that would be occupied by neighboring electrons of the surrounding classical atoms. Within the modified scheme that we propose here, the NMR chemical shifts agree well with full ab initio calculations.

As expected, full quantitative agreement cannot always be reached in the extreme case of those atoms directly in contact with the classically modeled region. We have investigated this situation by placing only a single water molecule in the QM sector, and modeling classically the surrounding solvent mol-

ecules, whose coordinates were taken from a fully quantum mechanical molecular dynamics simulation. The improvement that is also found for these situations shows that the repulsive potential, together with the QM/MM scheme, is capable of modeling a good part of the electronic interactions also in the QM/MM interface region.

The model fails for the polarization of the oxygen atom in the extreme case of a single molecule in the quantum region but it improves the results for oxygen atoms in water clusters.

The approach is validated by analyzing a system of a completely different structure, a crystal with strong NH \cdots N hydrogen bonds. The QM/MM implementation, in combination with the potential that replaces the Pauli repulsion, is capable of reproducing the full-quantum NMR chemical shift spectrum in good qualitative agreement.

Our tool can be used together with Car–Parrinello molecular dynamics simulations for obtaining the measurable averages over NMR chemical shifts for dynamically evolving systems. For doing so, one has to apply the same procedure as for the fully QM-based calculations of such systems, as done in ref 7. First, a molecular dynamics simulation has to be carried out for a sufficient time to let the system equilibrate, and subsequently, a number of representative configurations has to be extracted from the simulations as input for the QM/MM NMR chemical shift calculations. The required number of snapshots may vary depending on the considered system. For liquid and supercritical water, for instance, around one thousand proton chemical shifts turned out to yield a good statistics and to reproduce well the experimental results.⁷

A further project is the extension of the method to situations where the QM/MM boundary goes through a covalent bond. Preliminary calculations show that for such systems, both the special “dummy” pseudopotential that replaces the first MM atom as well as the Pauli repulsion potential need to be modified. We are working on a systematic improvement scheme for this kind of situations, which will be published soon.²⁰

Acknowledgment. We thank Michele Parrinello and Juerg Hutter for support and many very useful discussions. D.S. acknowledges financial support from the “DFG Sonderforschungsbereich 625”.

References and Notes

- (1) Brown, S.; Spiess, H. W. *Chem. Rev.* **2001**, *101*, 4125.
- (2) Mauri, F.; Pfrommer, B.; Louie, S. *Phys. Rev. Lett.* **1996**, *77*, 5300–5303.
- (3) Sebastiani, D.; Parrinello, M. *J. Phys. Chem. A* **2001**, *105*, 1951.
- (4) Jones, R. O.; Gunnarsson, O. *Rev. Mod. Phys.* **1989**, *61*, 689–746.
- (5) Mauri, F.; Pfrommer, B.; Louie, S. *Phys. Rev. Lett.* **1997**, *79*, 2340.
- (6) Yoon, Y.; Pfrommer, B.; Mauri, F.; Louie, S. *Phys. Rev. Lett.* **1998**, *80*, 3388.
- (7) Sebastiani, D.; Parrinello, M. *ChemPhysChem* **2002**, *3*, 675.
- (8) Pfrommer, B.; Mauri, F.; Louie, S. *J. Am. Chem. Soc.* **2000**, *122*, 123–129.
- (9) Goward, G.; Schuster, M. F.; Sebastiani, D.; Schnell, I.; Spiess, H. W. *J. Phys. Chem. B* **2002**, *106*, 9322.
- (10) Sherwood, P. In *Modern Methods and Algorithms of Quantum Chemistry*; Grotendorst, J., Ed.; NIC Series; John von Neumann Institute for Computing: Jülich, 2000; Vol. 1, pp 257–277.
- (11) Cui, Q.; Karplus, M. *J. Phys. Chem. B* **2000**, *104*, 3721–3743.
- (12) Cui, Q.; Karplus, M. *J. Chem. Phys.* **2000**, *112*, 1133.
- (13) Frisch, M. J.; Trucks, G. W.; Schlegel, H. B.; Gill, P. M. W.; Johnson, B. G.; Robb, M. A.; Cheeseman, J. R.; Keith, T.; Petersson, G. A.; Montgomery, J. A.; Raghavachari, K.; Al-Laham, M. A.; Zakrzewski, V. G.; Ortiz, J. V.; Foresman, J. B.; Peng, C. Y.; Ayala, P. Y.; Chen, W.; Wong, M. W.; Andres, J. L.; Replogle, E. S.; Gomperts, R.; Martin, R. L.; Fox, D. J.; Binkley, J. S.; Defrees, D. J.; Baker, J.; Stewart, J. P.; Head-Gordon, M.; Gonzalez, C.; Pople, J. A. *Gaussian 98*, revision A.7; Gaussian Inc.: Pittsburgh, PA, 1998.
- (14) Laio, A.; VandeVondele, J.; Rothlisberger, U. *J. Chem. Phys.* **2002**, *116*, 6941.
- (15) van Gunsteren, W.; Berendsen, H. *Computer code GROMOS96*.
- (16) Case, D. A.; Pearlman, D. A.; Caldwell, J. W.; T. E. C., III; Wang, J.; Ross, W. S.; Simmerling, C.; Darden, T.; Merz, K. M.; Stanton, R. V.; Cheng, A.; Vincent, J. J.; Crowley, M.; Tsui, V.; Gohlke, H.; Radmer, R.; Duan, Y.; Pitera, J.; Massova, I.; Seibel, G. L.; Singh, U. C.; Weiner, P.; Kollman, P. A. *Computer code AMBER*.
- (17) Car, R.; Parrinello, M. *Phys. Rev. Lett.* **1985**, *55*, 2471.
- (18) Hutter, J.; Marx, D.; Focher, P.; Tuckerman, M.; Andreoni, W.; Curioni, A.; Fois, E.; Rothlisberger, U.; Giannozzi, P.; Deutsch, T.; Alavi, A.; Sebastiani, D.; Laio, A.; VandeVondele, J.; Seitsonen, A.; Billeter, S.; Parrinello, M. *Computer code CPMD*, version 3.8.
- (19) Sebastiani, D.; Goward, G.; Schnell, I.; Spiess, H.-W. *J. Mol. Struct. (THEOCHEM)* **2003**, *625*, 283–288.
- (20) von Lilienfeld-Toal, O. A.; Tavernelli, I.; Rothlisberger, U.; Sebastiani, D. Manuscript in preparation.
- (21) Putrino, A.; Sebastiani, D.; Parrinello, M. *J. Chem. Phys.* **2000**, *113*, 7102.
- (22) Hohenberg, P.; Kohn, W. *Phys. Rev.* **1964**, *136*, B864.
- (23) Kohn, W.; Sham, L. J. *Phys. Rev.* **1965**, *140*, A1133.
- (24) Kutzelnigg, W. *Isr. J. Chem.* **1980**, *19*, 193.
- (25) Ditchfield, R. *J. Chem. Phys.* **1972**, *56*, 5688.
- (26) Keith, T. A.; Bader, R. F. W. *Chem. Phys. Lett.* **1993**, *210*, 223.
- (27) Berghold, G.; Mundy, C.; Romero, A.; Hutter, J.; Parrinello, M. *Phys. Rev. B* **2000**, *61*, 10040.
- (28) Sebastiani, D.; Goward, G.; Schnell, I.; Parrinello, M. *Comput. Phys. Commun.* **2002**, *147*, 707.
- (29) Martyna, G.; Tuckerman, M. *J. Chem. Phys.* **1999**, *110*, 1810.
- (30) Amovilli, C.; Mennucci, B. *J. Phys. Chem. B* **1997**, *101*, 1051–1057.
- (31) Gordon, M. S.; Freitag, M. A.; Bandyopadhyay, P.; Jensen, J. H.; Kairys, V.; Stevens, W. J. *J. Phys. Chem. A* **2001**, *105*, 293–307.
- (32) Cui, Q. *J. Chem. Phys.* **2002**, *117*, 4720–4728.
- (33) Jensen, J. H.; Gordon, M. S. *J. Chem. Phys.* **1998**, *108*, 4772–4782.
- (34) Zhang, Y.; Lee, T.-S.; Yang, W. *J. Phys. Chem.* **1999**, *110*, 46–54.
- (35) Silvestrelli, P.; Parrinello, M. *J. Chem. Phys.* **1999**, *111*, 3572.
- (36) Hartwigsen, C.; Goedecker, S.; Hutter, J. *Phys. Rev. B* **1998**, *58*, 3641.
- (37) Sprik, M.; Hutter, J.; Parrinello, M. *J. Chem. Phys.* **1996**, *105*, 1142.
- (38) Silvestrelli, P. L.; Bernasconi, M.; Parrinello, M. *Chem. Phys. Lett.* **1997**, *277*, 478–482.
- (39) Katrusiak, A. *Phys. Rev. Lett.* **1996**, *77*, 4366.
- (40) Sakane, S.; Yezdimer, E. M.; Liu, W.; Barriocanal, J. A.; Doren, D. J.; Woodb, R. H. *J. Chem. Phys.* **2000**, *113*, 2583–2593.
- (41) Tu, Y.; Laaksonen, A. *Chem. Phys. Lett.* **2000**, *329*, 283–288.
- (42) Modig, K.; Halle, B. *J. Am. Chem. Soc.* **2002**, *124*, 12031–12041.
- (43) Eisenberg, D.; Kauzmann, W. *The Structure and Properties of Water*; Clarendon: Oxford, U.K., 1969.
- (44) Walrafen, G. E. *Water. A Comprehensive Treatise*; Franks, F., Ed.; Plenum Press: New York, 1972; Vol. 1.
- (45) Stillinger, F. H. *Science* **1980**, *209*, 451.
- (46) Pickard, C. J.; Mauri, F. *Phys. Rev. B* **2001**, *63*, 245101.
- (47) Sebastiani, D.; Rothlisberger, U. In *Medicinal Quantum Chemistry*; Mannhold, R.; Kubiny, H.; Folkers, G., Series Eds.; Vol. 88 of *Methods and Principles in Medicinal Chemistry*; Wiley-VCH: Weinheim, Germany, 2003; pp 5–36.
- (48) Bayly, C. I.; Cieplak, P.; Cornell, W. D.; Kollman, P. A. *J. Phys. Chem.* **1993**, *97*, 10269.